# Polymorphic Control of $CsGaE_2$ (E = S, Se) Using Diorganyl Dichalcogenide Precursors

Zhaohong Sun,[a] Christopher P. Pakhanyan,[a] Usama Saleem,[b] Eitan I. Feldman,[c] Shaama Mallikarjun Sharada,[a,b] and Richard L. Brutchey*[a]

[a] Department of Chemistry, University of Southern California, Los Angeles, California 90089, United States. Email: brutchey@usc.edu
[b] Mork Family Department of Chemical Engineering and Materials Science, University of Southern California, Los Angeles, California 90089, United States.
[c] School of Natural Sciences and School of Engineering, Rice University, Houston, Texas 77005, United States.

**ABSTRACT:** Diorganyl dichalcogenides (R–E–E–R; R = organyl, E = S, Se, Te) are widely employed for the polymorphic control of diamond-like crystal structures owing to their tunable C–E bond reactivity. In this work, we extend their application to non-close-packed alkali metal-based chalcogenides by demonstrating the selective synthesis of $CsGaE_2$ (E = S, Se) polymorphs. Weaker C–E bonds or higher temperatures promote the formation of the thermodynamically stable *mC*64 phases, while stronger C–E bonds or lower temperatures allow for the isolation of the metastable *mC*16 phases. Heat-treatment studies reveal the pronounced metastability of $CsGaSe_2$-*mC*16 particles and the irreversible phase transition of $CsGaS_2$ analogous to its bulk counterpart.

Polymorphism, or the existence of multiple crystal structures for a single composition, significantly broadens the physical and chemical property landscape of solid-state materials. Many diamond-like chalcogenide semiconductors, such as zinc-blende ZnSe, chalcopyrite $Cu(In,Ga)Se_2$, and kesterite $Cu_2ZnSn(S,Se)_4$, with cubic-close-packed (ccp) cation/anion sublattices, can give rise to metastable wurtzite(-like) counterparts characterized by hexagonal-close-packed (hcp) sublattices.[1–17] Some of these metastable phases occupy high-temperature regions of thermodynamic phase diagrams, while others can only be kinetically trapped under specific reaction conditions and do not exist on bulk phase diagrams.[1] *Chimie douce* (soft-chemistry) synthesis has emerged as a powerful platform for accessing such metastable polymorphs, owing to kinetic control via precursor reactivity and phase stabilization by ligand passivation.

Among various precursors, diorganyl dichalcogenides (R–E–E–R, where R = Bn, Ph, Me, etc.; E = S, Se, Te) have proven particularly versatile in phase control due to their tunable C–E bond dissociation energies.[18–22] For each chalcogen type, $Bn_2E_2$ and $Ph_2E_2$ have weak and strong C–E bonds, making them more and less reactive, respectively, while alkyl R-groups result in intermediate reactivity. We previously showed that diphenyl diselenide ($Ph_2Se_2$) and dibenzyl diselenide ($Bn_2Se_2$) can selectively yield metastable wurtzite-like and thermodynamically preferred chalcopyrite $CuInSe_2$ nanocrystals, respectively, by controlling the formation of distinct binary copper selenide intermediates via different C–Se bond reactivities using a molecular programming approach.[5] This strategy has since been utilized to access a broad family of metastable multinary chalcogenides, such as wurtzite-like $Cu_2SnSe_3$ and $Cu_2ZnSnSe_4$.[2,3,11–13] Two

other metastable phases of $Cu_{2-x}Se$ nanocrystals—wurtzite and weissite—were synthesized using $Ph_2Se_2$ and/or didodecyl diselenide ($DD_2Se_2$), further showcasing their utility in accessing unconventional crystal structures.[23–25]

Beyond close-packed tetrahedral structures, the introduction of larger cations, such as alkali and alkaline-earth metals, can lower the lattice symmetry. This increases the diversity of possible structure types at fixed compositions and expands the landscape of potential metastable phases. For example, we recently reported the colloidal synthesis of metastable trigonal $Cu_2BaSnSe_4$ nanocrystals, which exhibit a more desirable band gap for solar light absorption than their thermodynamically stable orthorhombic counterparts.[26] While diorganyl dichalcogenides have been employed in the synthesis of alkali and alkaline-earth metal-based chalcogenide nanocrystals,[27–29] their utility in polymorphic control of this class of materials remains unexplored.

In this work, we investigate this using $CsGaE_2$ (E = S, Se) as a model system. Bulk $CsGaE_2$ has two polymorphs; that is, the low-temperature *mC*64 phase and the high-temperature *mC*16 phase (**Figure 1a**).[30,31] Both phases crystallize in a monoclinic *C*2/*c* space group, with "*mC*" denoting a base-centered monoclinic lattice followed by the number of atoms per unit cell.[30] The *mC*64 phase has a $TlGaSe_2$-type structure, characterized by two-dimensional layers of corner-sharing $[GaE_4]$ tetrahedra, separated by 8-coordinate $Cs^+$ cations; the *mC*16 phase crystallizes in $KFeS_2$-type, consisting of one-dimensional chains of edge-sharing $[GaE_4]$ tetrahedra, hexagonally packed among 8-coordinate $Cs^+$. The *mC*64 phase transitions to the *mC*16 phase upon heating to ~600 °C. For $CsGaSe_2$, this phase transition is reversible upon cooling.[30] For $CsGaS_2$, however, high pressure is required to reverse this transition.[31] Our density functional theory (DFT) calculations revealed that for both $CsGaSe_2$ and $CsGaS_2$, the bulk energy of the *mC*16 phase is only 0.01 eV/atom higher than the *mC*64 phase (**Table S1**), rendering them metastable but synthesizable via soft chemistry approaches. Such diverse polymorphic behavior makes $CsGaE_2$ a promising model system for study.

$CsGaE_2$ particles were synthesized by heating $Cs_2CO_3$, Ga(acetylacetonate)$_3$, and $R_2E_2$ (E = S, Se) precursors in oleylamine and oleic acid for 30 min. A degassing step at 140 °C for 30 min was performed before ramping to target temperatures to ensure the full dissolution and activation of precursors. The outcomes of representative control reactions are summarized as phase maps in **Figure 1b** and **c**, demonstrating successful polymorphic control of both $CsGaSe_2$ and $CsGaS_2$. Their crystal structures were characterized by powder X-ray diffraction (XRD) and Rietveld refinement (**Figure 2**),[32,33] with refined lattice parameters in close agreement with those of the reported bulk phases (**Table S2**).[30,31]

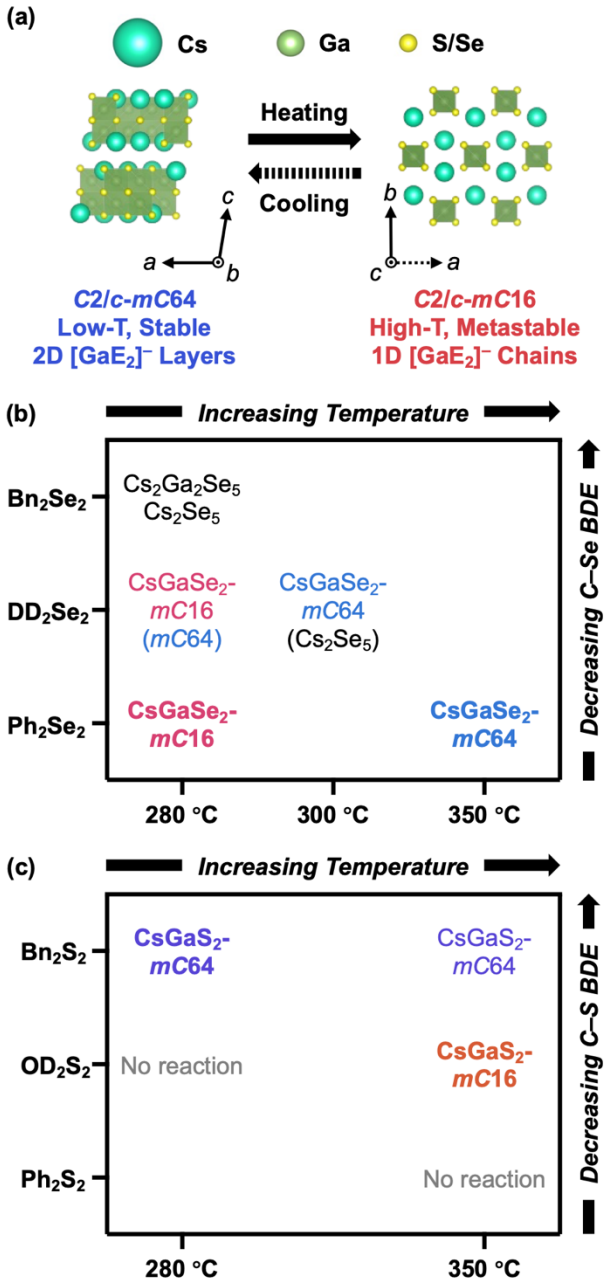


**Figure 1.** (a) Schematic illustration of $CsGaE_2$ (E = S, Se) polymorphs and their bulk phase transition behaviors. (b,c) $CsGaE_2$ phase maps with various $R_2E_2$ precursors and temperatures, demonstrating the soft-chemistry polymorphic control of (b) $CsGaSe_2$ and (c) $CsGaS_2$. Arrows demonstrate that both weaker C–E bonds and higher temperatures drive thermodynamic pathways to the stable *mC*64 phases. Minor products are shown in parentheses. Bolded products indicate those selected for detailed characterization. Powder XRD patterns of all other reaction products are provided in **Figure S1**.

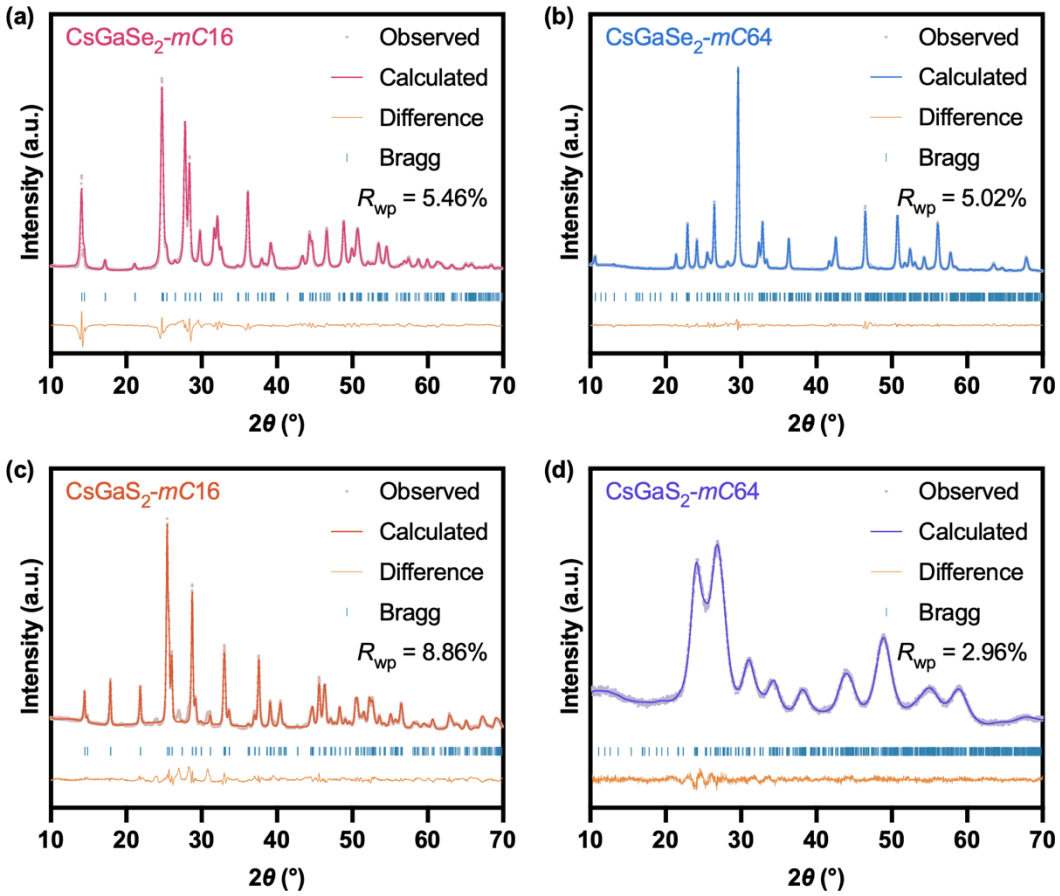


**Figure 2.** Rietveld refinements of the laboratory powder XRD patterns of (a) $CsGaSe_2$-*mC*16, (b) $CsGaSe_2$-*mC*64, (c) $CsGaS_2$-*mC*16, and (d) $CsGaS_2$-*mC*64, with $\lambda = 1.5406$ Å.

The use of $Ph_2Se_2$ at 280 °C yielded the metastable *mC*16 phase of $CsGaSe_2$ (**Figure 2a**). This temperature is well below the phase-transition threshold of $CsGaE_2$ (~600 °C), indicating a kinetically controlled formation pathway governed by precursor chemistry. In contrast, raising the reaction temperature to 350 °C produced the thermodynamically stable $CsGaSe_2$-*mC*64 phase (**Figure 2b**). Aliquot studies revealed direct nucleation of $CsGaSe_2$-*mC*16 by 280 °C, with no evidence of binary intermediates (**Figure S2a**). The *mC*16 phase remained metastable up to 350 °C but relaxed to *mC*64 *in situ* upon extended heating (>5 min), suggesting a temperature-driven thermodynamic pathway.

Attempts to synthesize $CsGaSe_2$-*mC*64 with $Bn_2Se_2$ at 280 °C yielded a mixture of $Cs_2Ga_2Se_5$ and $Cs_2Se_5$ (**Figure S1a**). $Cs_2Ga_2Se_5$ is more Se-rich and can also be obtained by reacting $CsGaSe_2$ with $Se^0$ in solid-state reactions,[34] whereas $Cs_2Se_5$ features unbranched $Se_5^{2-}$ chains, indicating "polymerization" of Se released from $Bn_2Se_2$.[35] Previous studies have shown that $Ph_2Se_2$ prefers the cleavage of weaker Se–Se bonds over stronger C–Se bonds, leading to the steady release of Se atoms.[36] In contrast, $Bn_2Se_2$ cleaves weaker C–Se bonds rather than stronger Se–Se bonds, producing elemental selenium ($Se^0$) as essentially a polymer of Se–Se bonds.[36] Such uncontrolled reactivity often yields $Se^0$ or polyselenide anions as side products. A similar trend was observed

in our copper selenide studies, where the klockmannite CuSe phase containing Se–Se bonds could be synthesized using $Bn_2Se_2$ but not $Ph_2Se_2$.[25] Taken together, these findings indicate that the highly reactive C–Se bond in $Bn_2Se_2$ is unsuitable for controlled $CsGaSe_2$ formation.

To further probe the reactivity trend of $R_2Se_2$, we tested didodecyl diselenide ($DD_2Se_2$), which possesses an intermediate C–Se bond strength. At 280 °C, the reaction yielded primarily the *mC*16 phase with minor reflections of *mC*64 (**Figure S1b**), suggesting that the weaker C–E bonds in $DD_2Se_2$ compared to $Ph_2Se_2$ tipped the balance toward the thermodynamic pathway. Increasing the temperature to 300 °C shifted the product phase to $CsGaSe_2$-*mC*64, although several reflections corresponding to $Cs_2Se_5$ were also detected (**Figure S1c**). Notably, this phase change induced by only a 20 °C temperature increase underscores the significant effect of temperature on precursor activation and phase determination.

The $R_2S_2$ analogs exhibited the same general trend, albeit with lower overall reactivity. The $Bn_2S_2$ precursor produced $CsGaS_2$-*mC*64 at both 280 °C and 350 °C (**Figure 2c** and **S1d**), whereas $Ph_2S_2$ yielded no crystalline product even at 350 °C (**Figure S1e**), consistent with its robust C–S bonds and low reactivity.[18,19] Di-*n*-octadecyl disulfide ($OD_2S_2$) was inert at 280 °C, as evidenced by recovery of crystalline $OD_2S_2$ (**Figure S1f**). Increasing the temperature to 350 °C enabled the activation of C–S bonds, yielding the metastable $CsGaS_2$-*mC*16 phase (**Figure 2d**). No binary intermediates were observed in the formation of either *mC*64 or *mC*16 phases (**Figure S2b** and **c**).

In summary, both $R_2Se_2$ and $R_2S_2$ precursors follow the reactivity trend of Ph < alkyl < Bn. More reactive precursors and higher temperatures drive thermodynamic pathways, favoring the *mC*64 phase or other Se-rich phases, whereas less reactive precursors and lower temperatures stabilize the metastable *mC*16 phase, or exhibit no reaction at all.

The resulting particle morphologies were characterized by scanning electron microscopy (SEM) or transmission electron microscopy (TEM). $CsGaSe_2$-*mC*16 crystallized into "knot"-like particles with average dimensions of 2.0 ± 0.6 μm ($N$ = 118), while some flakes were exfoliated from their surfaces (**Figure 3a**). $CsGaSe_2$-*mC*64 formed square plates with widths of 920 ± 330 nm ($N$ = 100) and thicknesses of 205 ± 89 nm ($N$ = 100, **Figure 3b**). $CsGaS_2$-*mC*16 exhibited rectangular rod or tablet morphologies, averaging 800 ± 260 nm ($N$ = 107) in length and 141 ± 97 nm ($N$ = 115) in width, with smaller particles growing on their surfaces (**Figure 3c**). In contrast, $CsGaS_2$-*mC*64 adopted an ultrathin nanowire morphology, with diameters of 5.1 ± 1.0 nm ($N$ = 245) and lengths of several hundred nm (**Figure 3d**). High-resolution TEM imaging revealed nanowire elongation along the [002] direction (**Figure S3**). These distinct particle morphologies highlight the significant effects of precursor chemistry and reaction temperature on crystallization pathways. Energy-dispersive X-ray spectroscopy (SEM-EDX) analysis revealed nearly stoichiometric $CsGaE_2$ compositions for all four phases (**Table S3** and **Figure S4**).

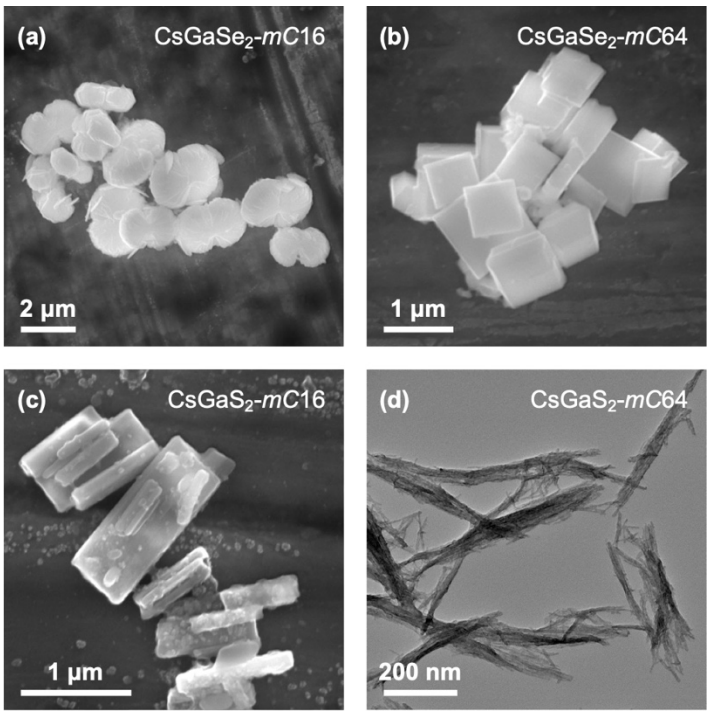


**Figure 3.** (a–c) SEM images of (a) $CsGaSe_2$-*mC*16, (b) $CsGaSe_2$-*mC*64, and (c) $CsGaS_2$-*mC*16 particles. (d) TEM image of $CsGaS_2$-*mC*64 nanowires.

Ultraviolet–visible (UV–vis) diffuse reflectance spectra of $CsGaE_2$ powders each exhibited a distinct absorption edge (**Figure S5**). The optical band gaps were determined using Tauc plots and the Kubelka–Munk function (**Figure S6**).[37] $CsGaSe_2$-*mC*16 and *mC*64 exhibited band gaps of 3.38 eV and 3.17 eV, respectively, while $CsGaS_2$-*mC*16 and *mC*64 returned band gaps of 4.09 and 4.19 eV, respectively. For each composition, both polymorphs revealed similar band gaps. $TlGaSe_2$-type $CsInSe_2$ nanocrystals isostructural to the *mC*64 polymorphs possess a narrower band gap of 2.98 eV.[27] The band gap trend of $CsInSe_2$ < $CsGaSe_2$-*mC*64 < $CsGaS_2$-*mC*64 can be rationalized by the absolute chemical hardness ($\eta$) values of $In^{3+}$ (13) < $Ga^{3+}$ (17) and $Se^{2-}$ (3.8) < $S^{2-}$ (4.1),[38] whereas size effects may also have contributed to the high band gap of $CsGaS_2$-*mC*64 ultrathin nanowires.

Finally, we investigated the metastability and thermal phase transition behavior of $CsGaE_2$. Solid powders were heated at 10 °C/min, held isothermally for 1 h, and then cooled to room temperature at the same rate (**Figure 4**). For bulk $CsGaSe_2$, a fully reversible phase transition occurs near 600 °C, where the high-temperature *mC*16 phase completely converts to the room-temperature *mC*64 phase upon cooling.[30] In contrast, the $CsGaSe_2$-*mC*16 particles exhibited significantly enhanced metastability. Heating to 700 °C followed by cooling did not induce any transition to the *mC*64 phase (**Figure 4a**). Raising the temperature to 850 °C resulted in only a partial transition, while treatment at 1000 °C was required for complete conversion to the *mC*64 phase. The persistence of the metastable phase can be attributed to the small crystallite size, as evidenced by the broad XRD reflections up to 850 °C, which increased the kinetic barrier preventing relaxation to the thermodynamically favored *mC*64 structure.[1] Bulk $CsGaS_2$ undergoes

an irreversible phase transition—the *mC*16 phase remains stable upon cooling to room temperature unless high pressure is applied.[31] The $CsGaS_2$-*mC*64 nanowires mirrored the bulk behavior, remaining in the *mC*16 phase after heating to 700 °C or 1000 °C (**Figure 4b**).

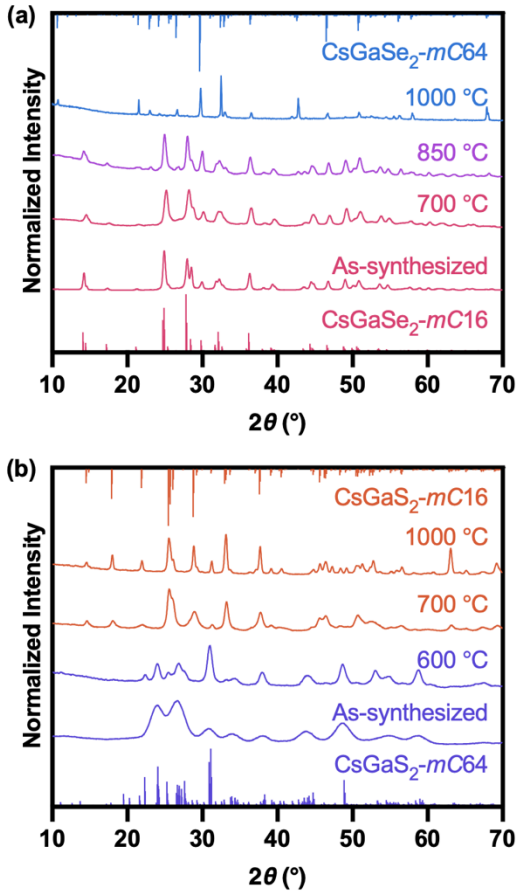


**Figure 4.** Room temperature powder XRD patterns illustrating phase transitions of (a) $CsGaSe_2$ and (b) $CsGaS_2$ upon heat treatment and cooling.

In conclusion, the polymorphic control of $CsGaE_2$ (E = S, Se) was achieved using diorganyl dichalcogenide ($R_2E_2$) precursors. The C–E bond strength and temperature played pivotal roles in governing reactivity and phase selectivity; that is, weaker C–E bonds or higher temperatures promoted thermodynamic pathways to the stable *mC*64 phase, while stronger C–E bonds or lower temperatures limited reactivity, enabling kinetic trapping of the metastable *mC*16 phase. Because $Bn_2Se_2$ contains overly labile C–Se bonds, it yielded undesired Se-rich phases ($Cs_2Ga_2Se_5$ and $Cs_2Se_5$), highlighting the importance of precisely controlling precursor reactivity in complex multinary systems. Phase-transition studies further revealed remarkable metastability in $CsGaSe_2$-*mC*16, which resisted conversion to the *mC*64 phase even upon extended heating, while $CsGaS_2$-*mC*64 followed bulk-like behavior with an irreversible transition to the *mC*16 phase. Overall, this work demonstrates the effectiveness of diorganyl dichalcogenides to molecularly program the

phase control of non-close-packed alkali metal-based chalcogenides, thereby expanding the synthetic toolbox for accessing novel functional semiconductors.

## ASSOCIATED CONTENT

### Supporting Information

The Supporting Information is available free of charge at

Experimental details; XRD patterns; TEM images; SEM-EDX data; UV–vis spectra; Tauc plots for band gap determination; DFT calculations; Rietveld refinements (PDF)

## AUTHOR INFORMATION

Corresponding Author

**Richard L. Brutchey** − *Department of Chemistry, University of Southern California, Los Angeles, California 90089, United States; orcid.org/0000-0002-7781-5596; Email: brutchey@usc.edu*

Authors

**Zhaohong Sun** – *Department of Chemistry, University of Southern California, Los Angeles, California 90089, United States; orcid.org/0000-0002-6176-0308*

**Christopher P. Pakhanyan** – *Department of Chemistry, University of Southern California, Los Angeles, California 90089, United States; orcid.org/0009-0009-4188-9567*

**Eitan I. Feldman** – *School of Natural Sciences and School of Engineering, Rice University, Houston, Texas 77005, United States*; *orcid.org/0009-0008-8643-1958*

**Usama Saleem** – *Mork Family Department of Chemical Engineering & Materials Science, University of Southern California, Los Angeles, California 90089, United States; orcid.org/ 0009-0001-4251-0688*

**Shaama Mallikarjun Sharada** – *Mork Family Department of Chemical Engineering & Materials Science, Department of Chemistry, University of Southern California, Los Angeles, California 90089, United States; orcid.org/0000-0001-7332-5373*

Notes

The authors declare no competing financial interest.

## ACKNOWLEDGMENTS

The work was supported by the U.S. Department of Energy, Office of Science, Basic Energy Sciences, under Award DE-FG02-11ER46826 to R.L.B. SEM, TEM, and EDX data presented in this article were acquired at the Core Center of Excellence in Nano Imaging at the University of Southern California. U.S. was supported by the Sloan Foundation and E. I. F. by USC's Summer Undergraduate Research Experience Program. The authors acknowledge USC's Center for Advanced Research Computing (CARC) for computational resources and support.

## REFERENCES

(1) Tappan, B. A.; Brutchey, R. L. Polymorphic Metastability in Colloidal Semiconductor Nanocrystals. *ChemNanoMat* **2020**, *6*, 1567–1588. https://doi.org/10.1002/cnma.202000406.
(2) Tappan, B. A.; Chu, W.; Mecklenburg, M.; Prezhdo, O. V.; Brutchey, R. L. Discovery of a Wurtzite-like $Cu_2FeSnSe_4$ Semiconductor Nanocrystal Polymorph and Implications for Related $CuFeSe_2$ Materials. *ACS Nano* **2021**, *15*, 13463–13474. https://doi.org/10.1021/acsnano.1c03974.
(3) Tappan, B. A.; Crans, K. D.; Brutchey, R. L. Formation Pathway of Wurtzite-like $Cu_2ZnSnSe_4$ Nanocrystals. *Inorg. Chem.* **2021**, *60*, 17178–17185. https://doi.org/10.1021/acs.inorgchem.1c02506.
(4) Tappan, B. A.; Horton, M. K.; Brutchey, R. L. Ligand-Mediated Phase Control in Colloidal $AgInSe_2$ Nanocrystals. *Chem. Mater.* **2020**, *32*, 2935–2945. https://doi.org/10.1021/acs.chemmater.9b05163.
(5) Tappan, B. A.; Barim, G.; Kwok, J. C.; Brutchey, R. L. Utilizing Diselenide Precursors toward Rationally Controlled Synthesis of Metastable $CuInSe_2$ Nanocrystals. *Chem. Mater.* **2018**, *30*, 5704–5713. https://doi.org/10.1021/acs.chemmater.8b02205.
(6) Wang, Y.-H. A.; Zhang, X.; Bao, N.; Lin, B.; Gupta, A. Synthesis of Shape-Controlled Monodisperse Wurtzite $CuIn_xGa_{1-x}S_2$ Semiconductor Nanocrystals with Tunable Band Gap. *J. Am. Chem. Soc.* **2011**, *133*, 11072–11075. https://doi.org/10.1021/ja203933e.
(7) Wang, J.-J.; Wang, Y.-Q.; Cao, F.-F.; Guo, Y.-G.; Wan, L.-J. Synthesis of Monodispersed Wurtzite Structure $CuInSe_2$ Nanocrystals and Their Application in High-Performance Organic−Inorganic Hybrid Photodetectors. *J. Am. Chem. Soc.* **2010**, *132*, 12218–12221. https://doi.org/10.1021/ja1057955.
(8) Norako, M. E.; Greaney, M. J.; Brutchey, R. L. Synthesis and Characterization of Wurtzite-Phase Copper Tin Selenide Nanocrystals. *J. Am. Chem. Soc.* **2012**, *134*, 23–26. https://doi.org/10.1021/ja206929s.
(9) Norako, M. E.; Brutchey, R. L. Synthesis of Metastable Wurtzite $CuInSe_2$ Nanocrystals. *Chem. Mater.* **2010**, *22*, 1613–1615. https://doi.org/10.1021/cm100341r.
(10) Li, H.; Zanella, M.; Genovese, A.; Povia, M.; Falqui, A.; Giannini, C.; Manna, L. Sequential Cation Exchange in Nanocrystals: Preservation of Crystal Phase and Formation of Metastable Phases. *Nano Lett.* **2011**, *11*, 4964–4970. https://doi.org/10.1021/nl202927a.
(11) Chen, S.; Zu, B.; Jin, Q.; Wu, X.; Xu, Z.; Wu, L. General Synthesis of Wurtzite Cu-Based Quaternary Selenide Nanocrystals via the Colloidal Method. *ACS Appl. Mater. Interfaces* **2025**, *17*, 24382–24389. https://doi.org/10.1021/acsami.5c04244.
(12) Wang, J.-J.; Hu, J.-S.; Guo, Y.-G.; Wan, L.-J. Wurtzite $Cu_2ZnSnSe_4$ Nanocrystals for High-Performance Organic–Inorganic Hybrid Photodetectors. *NPG Asia Mater.* **2012**, *4*, e2–e2. https://doi.org/10.1038/am.2012.2.
(13) Wang, J.; Liu, P.; Seaton, C. C.; Ryan, K. M. Complete Colloidal Synthesis of $Cu_2SnSe_3$ Nanocrystals with Crystal Phase and Shape Control. *J. Am. Chem. Soc.* **2014**, *136*, 7954–7960. https://doi.org/10.1021/ja501591n.

(14) Bang, S.; Liu, J.; Wang, B.; Perez, C. M.; Liu, T.-R.; Crans, K. D.; Sun, Z.; Strzelecki, A.; Prezhdo, O. V.; Shao, Y.-T.; Guo, X.; Brutchey, R. L. High-Pressure Phase Transition of Metastable Wurtzite-Like $CuInSe_2$ Nanocrystals. *Chem. Mater.* **2025**, *37*, 2611–2618. https://doi.org/10.1021/acs.chemmater.5c00152.

(15) Ren, H.; Wang, M.; Li, Z.; Laffir, F.; Brennan, G.; Sun, Y.; Stokes, K.; Geaney, H.; O'Reilly, E. J.; Gao, P.; Liu, N.; McCarthy, C.; Ryan, K. M. Synthesis and Characterization of $CuZnSe_2$ Nanocrystals in Wurtzite, Zinc Blende, and Core–Shell Polytypes. *Chem. Mater.* **2019**, *31*, 10085–10093. https://doi.org/10.1021/acs.chemmater.9b03063.

(16) Xue, D.; Jiao, F.; Yan, H.; Xu, W.; Zhu, D.; Guo, Y.; Wan, L. Synthesis of Wurtzite $Cu_2ZnGeSe_4$ Nanocrystals and Their Thermoelectric Properties. *Chem.—Asian J.* **2013**, *8*, 2383–2387. https://doi.org/10.1002/asia.201300425.

(17) Sun, Z.; Baluyot-Reyes, N.; Zamarripa, K.; Djurovich, P. I.; Thompson, M. E.; Brutchey, R. L. Polytypic Zn–(In,Ga)–Se Nanocrystals with Tunable Emission. *Nano Lett.* **2025**, *25*, 14310–14316. https://doi.org/10.1021/acs.nanolett.5c03311.

(18) Brutchey, R. L. Diorganyl Dichalcogenides as Useful Synthons for Colloidal Semiconductor Nanocrystals. *Acc. Chem. Res.* **2015**, *48*, 2918–2926. https://doi.org/10.1021/acs.accounts.5b00362.

(19) Guo, Y.; Alvarado, S. R.; Barclay, J. D.; Vela, J. Shape-Programmed Nanofabrication: Understanding the Reactivity of Dichalcogenide Precursors. *ACS Nano* **2013**, *7*, 3616–3626. https://doi.org/10.1021/nn400596e.

(20) Antunez, P. D.; Webber, D. H.; Brutchey, R. L. Solution-Phase Synthesis of Highly Conductive Tungsten Diselenide Nanosheets. *Chem. Mater.* **2013**, *25*, 2385–2387. https://doi.org/10.1021/cm400790z.

(21) Geisenhoff, J. Q.; Tamura, A. K.; Schimpf, A. M. Using Ligands to Control Reactivity, Size and Phase in the Colloidal Synthesis of $WSe_2$ Nanocrystals. *Chem. Commun.* **2019**, *55*, 8856–8859. https://doi.org/10.1039/C9CC03326B.

(22) Rhodes, J. M.; Jones, C. A.; Thal, L. B.; Macdonald, J. E. Phase-Controlled Colloidal Syntheses of Iron Sulfide Nanocrystals via Sulfur Precursor Reactivity and Direct Pyrite Precipitation. *Chem. Mater.* **2017**, *29*, 8521–8530. https://doi.org/10.1021/acs.chemmater.7b03550.

(23) Hernández-Pagán, E. A.; Robinson, E. H.; La Croix, A. D.; Macdonald, J. E. Direct Synthesis of Novel $Cu_{2-x}Se$ Wurtzite Phase. *Chem. Mater.* **2019**, *31*, 4619–4624. https://doi.org/10.1021/acs.chemmater.9b02019.

(24) Lord, R. W.; Fanghanel, J.; Holder, C. F.; Dabo, I.; Schaak, R. E. Colloidal Nanoparticles of a Metastable Copper Selenide Phase with Near-Infrared Plasmon Resonance. *Chem. Mater.* **2020**, *32*, 10227–10234. https://doi.org/10.1021/acs.chemmater.0c04058.

(25) Williamson, E. M.; Sun, Z.; Tappan, B. A.; Brutchey, R. L. Predictive Synthesis of Copper Selenides Using a Multidimensional Phase Map Constructed with a Data-Driven Classifier. *J. Am. Chem. Soc.* **2023**, *145*, 17954–17964. https://doi.org/10.1021/jacs.3c05490.

(26) Sun, Z.; Chen, Y.; Brutchey, R. L. Band Gap Engineering and Metastable Phase Discovery in $Cu_2BaSnS_{4-x}Se_x$ Nanocrystals via Topotactic Anion Exchange. *J. Am. Chem. Soc.* **2025**, *147*, 21219–21230. https://doi.org/10.1021/jacs.5c07324.
(27) Sun, Z.; Perez, C. M.; Prezhdo, O. V.; Brutchey, R. L. Colloidal $AInSe_2$ (A = K, Rb, Cs) Nanocrystals with Tunable Crystal and Band Structures. *ACS Nanosci. Au* **2024**, *4*, 381–390. https://doi.org/10.1021/acsnanoscienceau.4c00022.
(28) Sun, Z.; Pham, N.; Derakhshan, S.; Brutchey, R. L. Colloidal Synthesis of Ultrathin $KFeS_2$ and $RbFeS_2$ Magnetic Nanowires with Non-van Der Waals 1D Structures. *Chem. Sci.* **2025**, 10.1039.D5SC04592D. https://doi.org/10.1039/D5SC04592D.
(29) Pavel, M. R. S.; Santhiran, A.; Dalberg, S.; Rossini, A. J.; Vela, J. Alkaline Earth-Based Ternary Chalcogenide Nanocrystals: Cadmium- and Lead-Free Optical Materials. *ACS Nano* **2025**, *19*, 33413–33422. https://doi.org/10.1021/acsnano.5c10309.
(30) Friedrich, D.; Schlosser, M.; Pfitzner, A. Synthesis, Crystal Structure, and Physical Properties of Two Polymorphs of $CsGaSe_2$, and High-Temperature X-Ray Diffraction Study of the Phase Transition Kinetics. *Cryst. Growth Des.* **2016**, *16*, 3983–3992. https://doi.org/10.1021/acs.cgd.6b00532.
(31) Friedrich, D.; Schlosser, M.; Weihrich, R.; Pfitzner, A. Polymorphism of $CsGaS_2$—Structural Characterization of a New Two-Dimensional Polymorph and Study of the Phase-Transition Kinetics. *Inorg. Chem. Front.* **2017**, *4*, 393–400. https://doi.org/10.1039/C6QI00462H.
(32) *The Rietveld Method*; Young, R. A., Ed.; Oxford University Press: Oxford, 1993. https://doi.org/10.1093/oso/9780198555773.001.0001.
(33) Doebelin, N.; Kleeberg, R. Profex: A Graphical User Interface for the Rietveld Refinement Program *BGMN*. *J. Appl. Crystallogr.* **2015**, *48*, 1573–1580. https://doi.org/10.1107/S1600576715014685.
(34) Friedrich, D.; Schlosser, M.; Näther, C.; Pfitzner, A. In Situ X-Ray Diffraction Study of the Thermal Decomposition of Selenogallates $Cs_2[Ga_2(Se_2)_{2-x}Se_{2+x}]$ ( $x$ = 0, 1, 2). *Inorg. Chem.* **2018**, *57*, 5292–5298. https://doi.org/10.1021/acs.inorgchem.8b00324.
(35) Kretschmann, U.; Böttcher, P. Darstellung und Kristallstruktur des $Cs_2Se_5$ mit einer Anmerkung zum $Rb_2TeSe_4$. *Z. Naturforsch., B: J. Chem. Sci.* **1985**, *40*, 895–899. https://doi.org/10.1515/znb-1985-0708.
(36) Koziel, A. C.; Goldfarb, R. B.; Endres, E. J.; Macdonald, J. E. Molecular Decomposition Routes of Diaryl Diselenide Precursors in Relation to the Phase Determination of Copper Selenides. *Inorg. Chem.* **2022**, *61*, 14673–14683. https://doi.org/10.1021/acs.inorgchem.2c02042.
(37) Landi, S.; Segundo, I. R.; Freitas, E.; Vasilevskiy, M.; Carneiro, J.; Tavares, C. J. Use and Misuse of the Kubelka–Munk Function to Obtain the Band Gap Energy from Diffuse Reflectance Measurements. *Solid State Commun.* **2022**, *341*, 114573. https://doi.org/10.1016/j.ssc.2021.114573.
(38) Pearson, R. G. Absolute Electronegativity and Hardness: Application to Inorganic Chemistry. *Inorg. Chem.* **1988**, *27*, 734–740. https://doi.org/10.1021/ic00277a030.

TOC Graphic:

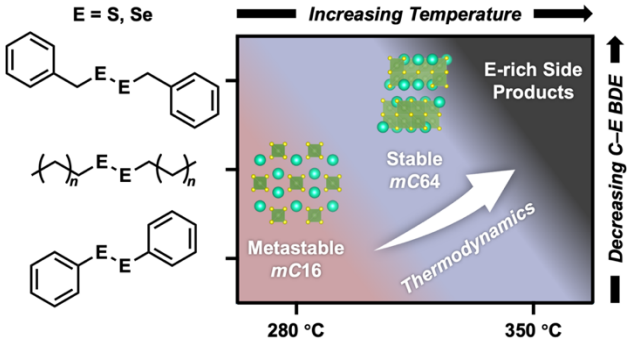
E = S, Se
Increasing Temperature
E-rich Side Products
Stable mC64
Metastable mC16
Thermodynamics
Decreasing C–E BDE
280 °C
350 °C